

PREPARED FOR SUBMISSION TO JCAP

Relativistic effects in Lyman- α forest

Vid Iršič,^a Enea Di Dio,^{b,c} Matteo Viel^{b,c}

^aThe Abdus Salam International Centre for Theoretical Physics, Strada Costiera 11, I-34151 Trieste, Italy

^bINAF - Osservatorio Astronomico di Trieste, Via G. B. Tiepolo 11, I-34143 Trieste, Italy

^cINFN-National Institute for Nuclear Physics, via Valerio 2, I-34127 Trieste, Italy

E-mail: virsic@ictp.it, enea.didio@oats.inaf.it, viel@oats.inaf.it

Abstract. We present the calculation of the Lyman-alpha (Lyman- α) transmitted flux fluctuations with full relativistic corrections to the first order. Even though several studies exist on relativistic effects in galaxy clustering, this is the first study to extend the formalism to a different tracer of underlying matter at unique redshift range ($z = 2 - 5$). Furthermore, we show a comprehensive application of our calculations to the Quasar-Lyman- α cross-correlation function. Our results indicate that the signal of relativistic effects can be as large as 30% at Baryonic Acoustic Oscillation (BAO) scale, which is much larger than anticipated and mainly due to the large differences in density bias factors of our tracers. We construct an observable, the anti-symmetric part of the cross-correlation function, that is dominated by the relativistic signal and offers a new way to measure the relativistic terms at relatively small scales. The analysis shows that relativistic effects are important when considering cross-correlations between tracers with very different biases, and should be included in the data analysis of the current and future surveys. Moreover, the idea presented in this paper is highly complementary to other techniques and observables trying to isolate the effect of the relativistic corrections and thus test the validity of the theory of gravity beyond the Newtonian regime.

Contents

1	Introduction	1
2	Ly-α absorption	2
3	Ly-α observable	3
3.1	Biases	6
4	2-point correlation function	7
4.1	Local term expansion in \mathcal{H}/k	12
4.2	Symmetric correlation function	15
4.3	Anti-symmetric correlation function	15
5	Conclusions	20
A	Angular power spectrum	22
B	CLASS modifications	23

1 Introduction

The last decade has witnessed an enormous progress in the cosmological investigation of the intergalactic medium (IGM) as probed by the Lyman- α forest (see [1, 2] for reviews). In particular, the Lyman- α forest is now a viable cosmological observable that can help in putting constraints on cosmological parameters and/or deviations from a standard scenario based on Cold Dark Matter (CDM) and a cosmological constant. More recently, the very large number of quasar spectra of the SDSS-III/BOSS (Sloan Digital Sky Survey-III/Baryon Oscillation Spectroscopic Survey) collaboration using a state-of-the-art analysis, has allowed to discover Baryonic Acoustic Oscillations (BAOs) in the transmitted Lyman- α flux at $z \sim 2.3$ [3, 4]: this spectacular confirmation of the cosmological nature of the Lyman- α forest was mainly made possible by exploiting the flux correlations in three dimensions out to large scales. Moreover, the one-dimensional analysis of the transmitted flux power has allowed to place the most stringent bounds on total neutrino mass and cold dark matter coldness by using spectra at high and low resolution [5–7].

The first steps have also been taken in measuring the cross-correlations between various different observables in the same volume of the survey. Such examples include the cross-correlations between the Lyman- α forest and Damped Lyman- α systems [8] and the Lyman- α forest and Quasars (QSOs) [9]. The first measurements measured the correlations up to the BAO scale and confirmed the location of the peak, however the error bars remain large. Nevertheless, the analysis was done on barely half of the

available data by the SDSS-III/BOSS survey and future generation of large-scale structure surveys (e.g. SDSS-IV/eBOSS [10], DESI [11], etc.) are going to improve on the precision of the measurements to a percent level thus forcing the theoretical models to match unprecedented demanding constraints in terms of accuracy.

However, as the observations move out to larger scales the validity of a simple Newtonian description starts to come into question. Recent years have seen a lot of effort put into understanding and possibly measuring the signal of relativistic effects and/or weak gravitational lensing in the 2-point statistics of the galaxy clustering, see e.g. [12–19]. Moreover, it has been speculated that the most powerful tool for such an analysis would be the cross-correlations between different galaxy populations [12, 13, 16, 18, 19]. The correlation of two differently biased tracers of the underlying matter field will, at least to the first order, boost the signal of the beyond-Kaiser effects relative to the difference in the density bias factors. Thus the larger the difference the stronger the signal. Unfortunately the difference in density bias factors among different galaxy populations is relatively small, and the idea has only received attention very recently.

On the other hand, the tracers such as Lyman- α forest or QSOs that are measured in the same survey volume by already existing surveys are very differently biased tracers. Exploiting this difference would boost the signal of the relativistic effects to a measurable level. Given the highly non-linear relation between the observed Lyman- α forest flux fluctuations and the underlying density field, one might question the ability to use the Lyman- α forest as a linear tracer. However, several studies have shown that on large scales Lyman- α forest behaves as any other local tracer and any deviations start to show up at smaller scales [20–22].

In this paper we compute the theoretical predictions for the QSO-Lyman- α cross-correlation function and show how the difference in the density biases of the two tracers boosts the signal of the relativistic effects to a 30% level. The paper is structured as follows: in Sections 2 and 3 we introduce the Lyman- α forest observable and derive the flux fluctuations using fully relativistic treatment. In Section 4 we apply the calculations to the QSO-Lyman- α cross-correlation function and present the results for both symmetric and anti-symmetric part. We conclude in Section 5.

2 Ly- α absorption

The Lyman- α forest is an absorption feature seen in the spectra of high redshift QSO and galaxies and is a unique tracer of the underlying matter distribution in the redshift range of $z = 2 - 5$.

When the light from a distant QSO passes through the intergalactic medium (IGM), the neutral hydrogen along the line of sight will cause absorption of the QSO continuum by the redshifted Lyman- α (121.565 nm) resonance line. The collection of this absorption lines blend into one feature called the Lyman- α forest. In fact it is more correct to think of the Lyman- α forest as being caused by continuous absorption of the mildly fluctuating density of the IGM.

Observed transmission of the flux is thus a tracer of the baryon distribution of the IGM and one of the successes of the Lyman- α in the last few years has been to establish it as a precision cosmology probe.

The photons' absorption due to Lyman- α is described by the differential equation

$$d \ln \mathcal{N}_\gamma = -A n_{\text{HI}} \phi(E, E_\alpha) dt \quad (2.1)$$

where E_α is the Lyman- α absorption line, \mathcal{N}_γ the photon occupation number, t the proper time in absorption HI rest frame and n_{HI} the number density of neutral hydrogen. A is a physical constant derived from Einstein coefficients and given by $A = e^2 f_\alpha / 4 \varepsilon_0 m_e$, where e is the electron charge, ε_0 is vacuum permittivity, m_e electron mass and $f_\alpha = 0.4164$ oscillation strength of the Lyman- α transition. The integral of the absorption line profile ($\phi(E, E_\alpha)$) over the energy is normalized to the unity. We define the optical depth as

$$\tau \equiv \int_{\text{light-cone}} d \ln \mathcal{N}_\gamma. \quad (2.2)$$

The above definition agrees with the non-relativistic result in the appropriate limit.

3 Ly- α observable

On large scales we can work under the approximation that $\phi(E, E_\alpha) = \delta_D(E - E_\alpha)$. Hence, we neglect thermal broadening which affects scales of $10 h^{-1}$ Mpc. This approximation is valid as long as we are interested in large scale correlations. Therefore, our observable is the transmitted flux fraction F , i.e. the photon occupation number observed normalized with the emitted one, which yields to

$$F = e^{-\tau}, \quad (3.1)$$

in terms of the measured angle¹ \mathbf{n} and redshift z , corresponding to the shift in the Lyman- α spectrum (i.e. $1 + z = E_\alpha/E$), namely $F(\mathbf{n}, z)$. One can define the fluctuations of the transmitted flux as

$$\delta_F(\mathbf{n}, z) \equiv \frac{F(\mathbf{n}, z)}{\langle F(\mathbf{n}, z) \rangle} - 1, \quad (3.2)$$

where $\langle . \rangle$ denotes the angular mean at fixed observed redshift z .

On large scales, we can linearize the relation between the transmitted flux and the optical depth and express the observable quantity as

$$\delta_F(\mathbf{n}, z) = -(\tau(\mathbf{n}, z) - \langle \tau(\mathbf{n}, z) \rangle) \equiv -\delta\tau(\mathbf{n}, z). \quad (3.3)$$

The linearization of the exponential in Eq. (3.1) might question the validity of the perturbative approach. Nevertheless, as shown in section 3.1, one can expand perturbatively the transmitted flux F in terms of the optical depth τ by introducing some bias factors which encode the effect of the mode coupling.

¹We follow the notation of Ref. [23], where \mathbf{n} denotes the direction of propagation of the photon. Hence the measured angle is $-\mathbf{n}$, but for sake of simplicity will refer to \mathbf{n} as argument of the observable quantities.

From Eqs. (2.1) and (2.2) we obtain

$$\begin{aligned}\tau(\mathbf{n}, z) &= -A \int n_{\text{HI}} \delta_D(E - E_\alpha) dt = -A \int n_{\text{HI}} \delta_D(E^{\text{obs}}(1+z) - E_\alpha) dt \\ &= -A \int \frac{n_{\text{HI}}}{E^{\text{obs}}} \delta_D\left((1+z) - \frac{E_\alpha}{E^{\text{obs}}}\right) \frac{dt}{dz} dz = -A n_{\text{HI}} \frac{1+z}{E_\alpha} \frac{dt}{dz}\end{aligned}\quad (3.4)$$

where all quantities are evaluated at $1+z = E_\alpha/E_{\text{obs}}$ and the suffix 'obs' denotes quantities evaluated with respect to the observer rest frame and t is the proper time² in the photons absorption frame.

In this section we aim to derive Eq. (3.3) to first order in perturbation theory. As long as we describe observable quantities, we have the freedom to work in any gauge without loss of generality. We choose to work in Newtonian gauge $d\tilde{s}^2 = a^2 ds^2$, where a is the scale factor of the universe and

$$ds^2 = -(1 + 2\Psi) d\eta^2 + (1 - 2\Phi) \delta_{ij} dx^i dx^j \quad (3.5)$$

is the conformal metric, where the metric perturbations Ψ and Φ are the Bardeen potentials. From Eq. (3.4), we need to compute $\frac{dt}{dz}$ to first order in perturbation theory

$$\begin{aligned}\frac{dt}{dz} &= \frac{dt}{d\eta} \frac{d\eta}{dz} = \frac{dt}{d\eta} \frac{d\eta}{dz} = \frac{1+\Psi}{1+\bar{z}} \left(\frac{d\bar{z}}{d\eta} + \frac{d\delta z}{d\eta} \right)^{-1} \\ &= \frac{1+\Psi}{1+\bar{z}} \left(\frac{d\bar{z}}{d\eta} \left(1 + \frac{\delta z}{1+z} \right) + (1+z) \frac{d}{d\eta} \left(\frac{\delta z}{1+z} \right) \right)^{-1} \\ &= -\frac{1+\Psi}{\mathcal{H}(\bar{z})(1+\bar{z})^2} \left[1 - \frac{\delta z}{1+z} + \frac{1}{\mathcal{H}} \frac{d}{d\eta} \left(\frac{\delta z}{1+z} \right) \right] \\ &= -\frac{1}{\mathcal{H}(1+z)^2} \left[1 + \Psi + \left(1 - \frac{\dot{\mathcal{H}}}{\mathcal{H}^2} \right) \frac{\delta z}{1+z} + \frac{1}{\mathcal{H}} \frac{d}{d\eta} \left(\frac{\delta z}{1+z} \right) \right] \\ &= -\frac{1}{\mathcal{H}(1+z)^2} \left[1 + \Psi + \left(1 - \frac{\dot{\mathcal{H}}}{\mathcal{H}^2} \right) \frac{\delta z}{1+z} + \mathbf{n} \cdot \mathbf{v} + \mathcal{H}^{-1} \partial_r \mathbf{n} \cdot \mathbf{v} + \mathcal{H}^{-1} \dot{\Phi} \right], \quad (3.6)\end{aligned}$$

where $\mathcal{H} = \dot{a}/a$ is the comoving Hubble parameter and a dot denotes the derivative with respect to the conformal time η . We have also introduced the unperturbed redshift \bar{z} by expanding the observed redshift as $z = \bar{z} + \delta z$. In general, in this work, we will denote with an overbar background quantities in perturbation theory. In the last equality we have assumed that sources move along geodesic

$$\mathbf{n} \cdot \dot{\mathbf{v}} + \mathcal{H} \mathbf{n} \cdot \mathbf{v} - \partial_r \Psi = 0, \quad (3.7)$$

and used

$$\frac{\delta z}{1+z} = - \left(\Psi + \mathbf{n} \cdot \mathbf{v} + \int_{\eta}^{\eta_o} (\dot{\Psi} + \dot{\Phi}) d\eta' \right), \quad (3.8)$$

²We prefer not to denote the proper time with τ to avoid confusion with the optical depth.

which is derived from geodesic equation. We remind that the physical density of HI, i.e. $n_{\text{HI}}(z)$ in Eq. (3.4), is related to the density computed in perturbation theory to first order as

$$n_{\text{HI}}(z) = \bar{n}_{\text{HI}}(z) \left(1 - \frac{d \ln \bar{n}_{\text{HI}}}{dz} \delta z + \delta_{\text{HI}} \right). \quad (3.9)$$

The second term in the brackets describes the source evolution and it is often parametrized through the evolution bias

$$f_{\text{evo}} \equiv \frac{\partial \ln(a^3 \bar{n}_{\text{HI}})}{\mathcal{H} \partial \eta} = 3 - (1+z) \frac{d \ln \bar{n}_{\text{HI}}}{dz}. \quad (3.10)$$

Finally, we find

$$\begin{aligned} \tau(\mathbf{n}, z) = \bar{\tau}(z) & \left[1 + \delta_{\text{HI}}^{\text{sync}} + \mathcal{H}^{-1} \partial_r \mathbf{n} \cdot \mathbf{v} - \left(2 + \frac{\dot{\mathcal{H}}}{\mathcal{H}^2} - f_{\text{evo}} \right) \frac{\delta z}{1+z} \right. \\ & \left. + \mathbf{n} \cdot \mathbf{v} + \Psi + \mathcal{H}^{-1} \dot{\Phi} + (f_{\text{evo}} - 3) \mathcal{H} v \right]. \end{aligned} \quad (3.11)$$

where

$$\bar{\tau}(z) \equiv \frac{A}{E_\alpha \mathcal{H}} \frac{\bar{n}_{\text{HI}}}{(1+z)} \quad (3.12)$$

and v is the (gauge invariant) velocity potential in Newtonian gauge defined through $\mathbf{v} = -\nabla v$. We have also expressed the density perturbation in synchronous gauge, through $\delta^{\text{sync}} = \delta + (3 - f_{\text{evo}}) \mathcal{H} v$.

The unperturbed optical depth $\bar{\tau}$ can be rewritten as ([22]):

$$\bar{\tau}(z) = \frac{A \bar{n}_{\text{HI}}}{E_\alpha H} \approx 1.27 \times \frac{10^{-12} \text{s}^{-1}}{\Gamma_{\gamma, \text{HI}}} \left(\frac{X}{0.75} \right)^2 \left(\frac{T_0}{10^4 \text{K}} \right)^{-0.7} \frac{\omega_{b,0}^2}{h} \frac{H_0}{H} (1+z)^6, \quad (3.13)$$

where T_0 is the mean temperature of the gas and we have used the mass fraction of neutral hydrogen through the photo-ionization equilibrium

$$n_{\text{HI}} = n_H^2 \frac{\alpha(T)}{\Gamma_{\gamma, \text{HI}}} = \frac{X^2 \rho_b^2}{m_H^2} \frac{\alpha(T)}{\Gamma_{\gamma, \text{HI}}}. \quad (3.14)$$

where $\Gamma_{\gamma, \text{HI}}$ is the photo-ionization rate, X is the hydrogen mass fraction, n_H is the hydrogen number density, m_H is the hydrogen mass, ρ_b is the baryon energy density and the recombination rate $\alpha(T)$ is given by

$$\alpha(T) = \alpha_0 \left(\frac{T}{10^4 \text{K}} \right)^{-0.7}, \quad (3.15)$$

where $\alpha_0 = 4.3 \times 10^{-13} \text{s}^{-1} \text{cm}^3$.

In this work we consider the Planck best fit cosmological parameters [24], namely $\omega_{b,0} = 0.022$, $h = 0.67$ and the astrophysical parameters $T_0 = 1.47088 \times 10^4 \text{K}$, $X = 0.75$ and $\Gamma_{\gamma, \text{HI}} = 10^{-12} \text{s}^{-1}$. With these parameters Eq. (3.13) reduces to

$$\bar{\tau}(z) \approx 7 \times 10^{-4} \frac{(1+z)^6}{E(z)} \quad (3.16)$$

with $E(z) = H(z)/H_0$.

3.1 Biases

In the previous section we have computed the optical depth $\tau(z)$ to first order in perturbation theory. However, the exponential (3.1) introduces a mode coupling that we neglect by linearizing this expression. In the context of the relativistic corrections beyond simple Kaiser approximation this is valid since the terms themselves are small. Indeed, they are suppressed at least by a factor \mathcal{H}/k . At the Hubble scale, $\mathcal{H} \sim k$, we expect relativistic corrections to be of the order of magnitude of density perturbations. Anyway both newtonian and relativistic terms are about 10^{-5} at the Hubble scale and our approximation can still be applied. However, on sub-Hubble scales, the density and redshift-space distortions terms are more prominently affected by the non-linear relation. To compensate for that we change our predicted values of density and velocity biases with the values suggested by the observations.

Therefore to correctly describe the transmitted flux fluctuation we change the density and velocity-gradient bias factors predicted by the linear theory with the observed bias factors

$$\delta_F(\mathbf{n}, z) = b_\alpha \delta^{\text{sync}} + b_v \mathcal{H}^{-1} \partial_r \mathbf{n} \cdot \mathbf{v} - \bar{\tau}(z) \left[- \left(2 + \frac{\dot{\mathcal{H}}}{\mathcal{H}^2} \right) \frac{\delta z}{1+z} + \mathbf{n} \cdot \mathbf{v} + \Psi + \mathcal{H}^{-1} \dot{\Phi} - 3\mathcal{H}v \right]. \quad (3.17)$$

The first two terms correspond to a simple Kaiser approximation for the Lyman- α forest tracer, while the terms in the square bracket describe the relativistic corrections. Note that the velocity-gradient bias different than unity is the result of the redshift space distortion acting on the optical depth, before taking the non-linear transformation to the observable which is the flux, and it is not to be interpreted as a violation of the equivalence principle. This result is known and widely used in the literature [20–22, 25].

In a relativistic framework one has to define the bias parameters with respect the density, and redshift space distortions for Lyman- α forest tracer, in a specific gauge. Indeed, if on small scales the differences between different gauges are generally suppressed by a factor $(\mathcal{H}/k)^2$, on large scales the gauge choice becomes relevant and it might introduce some spurious k -dependences in the bias factors.

However they do not affect the main results of our work which is determined by terms suppressed only by \mathcal{H}/k . Our choice to apply density bias b_α in synchronous comoving gauge is well justified from the assumption that the tracer and the underlying density perturbation experience the same gravitational field and they move with the same velocity. Hence in their rest frame we can apply the linear bias prescription. In the standard approach the velocity-gradient bias is applied to the Kaiser term, and is derived using Newtonian relation between time derivative of density perturbation and peculiar velocity. If Cold Dark Matter (CDM) is the only species which contributes to energy-momentum tensor perturbations, this relation is equivalent to the linearized Einstein equation provided that the density perturbation is expressed in the synchronous and velocity in the newtonian gauge. Therefore, to be consistent with standard analysis we used velocity-gradient bias in newtonian gauge.

In this work we consider the Lyman- α density bias evolution as suggested by the observations ([3, 4, 21, 26])

$$b_\alpha(z) = b_\alpha(z = 2.5) \left(\frac{1+z}{3.5} \right)^{2.9} \quad (3.18)$$

with $b_\alpha(z = 2.5) = -0.15$. For the velocity-gradient bias of the Lyman- α forest we follow the recent work using simulations ([20]) which gives:

$$b_v \equiv \frac{\beta_\alpha(z)b_\alpha(z)}{f(z)}, \quad \beta_\alpha(z) = \beta_\alpha(z = 2.5) \left(\frac{1+z}{3.5} \right)^{-0.86}, \quad (3.19)$$

with the value at the mean redshift $\beta_\alpha(z = 2.5) = 1.36$, and $f = d \ln \delta / d \ln a$ is the growth rate factor. In addition we have a vanishing evolution factor for Lyman- α forest, i.e. $f_{\text{evo}} = 0$ in Eq. (3.17). Strictly speaking this is not equivalent to zero by definition, since gas is in some thermal excited state, but the correction to the evolution bias of the IGM is very small ($< 10^{-7}$).

4 2-point correlation function

In the previous section we have derived the Lyman- α forest observable. Now we are interested in studying the 2-point function of the correlation between Ly- α and QSOs. Namely

$$\xi_{Q\alpha}(z_1, z_2, \theta) = \langle \Delta_Q(\mathbf{n}_1, z_1) \delta_F(\mathbf{n}_2, z_2) \rangle \quad (4.1)$$

where $\cos \theta = \mathbf{n}_1 \cdot \mathbf{n}_2$ and $\Delta_Q(\mathbf{n}, z)$ is the QSO number counts. The number counts for discrete tracers has been derived in [23, 27] in galaxy clustering framework. Nevertheless their results can be applied as well to QSOs, just considering the appropriate bias factors,

$$\begin{aligned} \Delta_Q(\mathbf{n}, z) = & b_Q \delta^{\text{sync}} + (5s - 2)\Phi + \Psi + \frac{1}{\mathcal{H}} \left[\dot{\Phi} + \partial_r(\mathbf{n} \cdot \mathbf{v}) \right] + (f_{\text{evo}} - 3) \mathcal{H}v \\ & + \left(\frac{\dot{\mathcal{H}}}{\mathcal{H}^2} + \frac{2 - 5s}{r_S \mathcal{H}} + 5s - f_{\text{evo}} \right) \left(\Psi + \mathbf{n} \cdot \mathbf{v} + \int_0^{r_S} dr (\dot{\Phi} + \dot{\Psi}) \right) \\ & + \frac{2 - 5s}{2r_S} \int_0^{r_S} dr \left[2 - \frac{r_S - r}{r} \Delta_\Omega \right] (\Phi + \Psi). \end{aligned} \quad (4.2)$$

Differently from Lyman- α forest, single tracer number counts include a cosmic magnification contribution and a magnification bias parameter s defined as

$$s = - \frac{2}{5} \frac{\partial \ln \bar{n}(z, \ln L)}{\partial \ln L} \Big|_{\bar{L}} \quad (4.3)$$

where \bar{L} denotes the threshold luminosity of the survey and \bar{n} is the background number density. Similarly, the evolution bias factor of QSOs is related to the QSO number density distribution (see Eq. (3.10)). To derive both bias parameters we have used a

fitting model for Quasar Luminosity Function used in BOSS DR9 data analysis [28]. The assumed threshold absolute magnitude was $\bar{M} = -24.5$. The derived values for the magnification and evolution bias factors are $s = 0.295319$ and $f_{\text{evo}} = 5.7999$.

For the QSO density bias factor (b_Q) we use the semi-empirical relation derived by [29, 30]:

$$b_Q(z) = 0.53 + 0.289(1+z)^2 \quad (4.4)$$

The empirical relation fits the observed data very well at lower redshifts and can be safely extrapolated to our mean redshift of $z = 2.5$, giving a value of $b_Q(z = 2.5) = 4$, which is a bit high, but in agreement with independent observations at higher redshifts [9, 31].

In general, it is always possible to express the 2-point correlation function in terms of angular power spectra $C_\ell(z_1, z_2)$ as

$$\xi(z_1, z_2, \theta) = \frac{1}{4\pi} \sum_{\ell} (2\ell + 1) C_\ell(z_1, z_2) P_\ell(\cos \theta) , \quad (4.5)$$

where P_ℓ denote the Legendre polynomials. In appendix A we introduce the corresponding angular power spectra. Since we are mainly interested in the 1-dimensional correlation function along the radial direction a direct evaluation of Eq. (4.1) is simpler and more intuitive than passing through Eq. (4.5). Nevertheless, we prefer to use Eq. (4.5) to handle the integrated terms (cosmic magnification, integrated Sachs-Wolfe, Shapiro time-delay) and take advantages of CLASS code [32, 33], whose modified transfer functions are shown in appendix B, than rely on approximations.

For the 1-dimensional radial correlation, Eq. (4.1) reduces to a function of two redshifts z_1 and z_2 . It is then convenient to re-express them as a redshift separation between the two source positions $\Delta z = z_1 - z_2$ and a mean redshift $z_{\text{mean}} = (z_1 + z_2)/2$. By assuming a fiducial model we can always map the redshift separation in terms of comoving separation as $x(z_1, z_2) \equiv r(z_1) - r(z_2)$, where

$$r(z) = \int_0^z \frac{dz'}{H(z')} \quad (4.6)$$

is the unperturbed comoving distance and

$$H^2(z) = H_0^2 (a^{-3}\Omega_m + a^{-2}\Omega_K + \Omega_\Lambda) . \quad (4.7)$$

We remark that to first order in perturbation theory it is enough to use the background unperturbed redshift-distance relation Eq. (4.6). Because, in general, sources are not homogeneously distributed along the redshift, the 1-dimensional correlation function will not depend only on the absolute value of Δz , or $x(z_1, z_2)$, but on its sign as well.

Ideally, since the pure radial correlation is described by a single line of sight, the light emitted by a QSO at high redshift would be partially absorbed by the IGM at lower redshift and it will generate the Lyman- α forest absorption lines. This situation is clearly a violation of the photon number conservation assumption on which the derivation (see for instance Ref. [23, 27]) of number count observable for discrete tracers is based. Nevertheless in our work we never consider this situation and we assume that the two

tracers, Lyman- α forest and QSO are correlated gravitationally only. This assumption is consistent with what is done in observations, where the correlation between the Lyman- α forest and the QSO, which produces the absorption lines, is not considered. An other issue is due to the fact that light emitted by a QSO at high redshift would be affected also by the gravitational potential generated by the Lyman- α forest through the cosmic magnification effect. Being the Lyman- α forest and the QSO on the same line of sight, the impact parameter of the light deflection vanishes and we can not anymore considered it in the weak lensing regime. Since, in any case, exact radial correlation are not taken into consideration we neglect this effect and we describe it as a weak lensing phenomenon. Let us also stress that these possible issues are completely relieved once we consider the dipole with respect to the angle β defined in Fig. 1. Indeed by averaging over all angles the contribution of one single direction has not weight in the integral and its contribution should be negligible. We leave the analysis of the dipole of the correlation function to a future work.

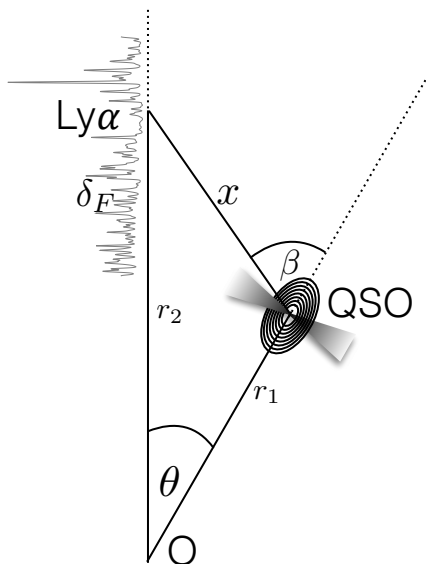


Figure 1. The figure illustrates the correlation between Quasars and Lyman- α forest. The comoving distances of the sources from the observer are denoted by r_1 and r_2 , while x refers to the comoving separation between them.

We compute then the full relativistic 2-point correlation function

$$\xi_{Q\alpha} = \xi_{Q\alpha}^{\text{newt}} + \xi_{Q\alpha}^{\text{magnification}} + \xi_{Q\alpha}^{\text{relativistic}} \quad (4.8)$$

where we dropped the dependence on Δz and z_{mean} for simplicity. We start by introducing the primordial curvature power spectrum through

$$\langle R_{\text{in}}(\mathbf{k}) R_{\text{in}}(\mathbf{k}') \rangle = (2\pi)^3 \delta_D^{(3)}(\mathbf{k} + \mathbf{k}') P_R(k) \quad (4.9)$$

and we write any first order variable X in terms of transfer functions normalized with the primordial curvature as

$$X(\mathbf{k}, \eta) = T_X(k, \eta) R_{\text{in}}(\mathbf{k}) . \quad (4.10)$$

Then, by computing the different contributions we find

$$\begin{aligned} \xi_{Q\alpha}^{\text{newt}} &\equiv \langle [b_Q \delta + \mathcal{H}^{-1} \partial_r(\mathbf{n} \cdot \mathbf{v})](\mathbf{n}, z_1) [b_\alpha \delta + b_v \mathcal{H}^{-1} \partial_r(\mathbf{n} \cdot \mathbf{v})](\mathbf{n}, z_2) \rangle \\ &= b_Q(z_1) b_\alpha(z_2) \int \frac{dk}{2\pi^2} k^2 T_\delta(k, \eta_1) T_\delta(k, \eta_2) P_R(k) j_0(kx) \\ &\quad + b_v(z_2) \int \frac{dk}{2\pi^2} \frac{k^4}{\mathcal{H}(z_1) \mathcal{H}(z_2)} T_v(k, \eta_1) T_v(k, \eta_2) P_R(k) \\ &\quad \times \left[\frac{1}{5} j_0(kx) - \frac{4}{7} j_2(kx) + \frac{8}{35} j_4(kx) \right] \\ &\quad + \int \frac{dk}{2\pi^2} k^3 P_R(k) \left[\frac{b_Q(z_1) b_v(z_2)}{\mathcal{H}(z_2)} T_\delta(k, \eta_1) T_v(k, \eta_2) + \frac{b_\alpha(z_2)}{\mathcal{H}(z_1)} T_v(k, \eta_1) T_\delta(k, \eta_2) \right] \\ &\quad \times \left[-\frac{1}{3} j_0(kx) + \frac{2}{3} j_2(kx) \right] \end{aligned} \quad (4.11)$$

where $x = x(z_1, z_2)$, and we allow for redshift dependent bias factors, while we have implicitly assumed that these are scale independent. Nevertheless a generalization to scale dependence bias factor would be straight forward. We define the correlation function induced by cosmic magnification as follows

$$\xi_{Q\alpha}^{\text{magnification}} \equiv \left\langle \left[\frac{5s-2}{2r} \int_0^r dr' \left[\frac{r-r'}{r'} \Delta_\Omega \right] (\Phi + \Psi) \right] (\mathbf{n}, z_1) [b_\alpha \delta + b_v \mathcal{H}^{-1} \partial_r(\mathbf{n} \cdot \mathbf{v})](\mathbf{n}, z_2) \right\rangle . \quad (4.12)$$

Because of the integral along the line of sight this expression can not be written in a simple form like Eq. (4.11), unless we adopt Limber approximation [34]. We therefore prefer to compute explicitly this contribution through Eq. (4.5). We define the relativistic contribution as follows

$$\begin{aligned} \xi_{Q\alpha}^{\text{relativistic}} &\equiv \langle \Delta_Q(\mathbf{n}, z_1) \delta_F(\mathbf{n}, z_2) \rangle - \xi_{Q\alpha}^{\text{newt}} - \xi_{Q\alpha}^{\text{magnification}} \\ &\equiv \xi_{Q\alpha}^{\text{Doppler}} + \xi_{Q\alpha}^{\text{potential}} + \xi_{Q\alpha}^{\text{non-local}} \end{aligned} \quad (4.13)$$

where we have a Doppler term³

$$\begin{aligned}
\xi_{Q\alpha}^{\text{Doppler}} &\equiv \langle [b_Q \delta + \mathcal{H}^{-1} \partial_r(\mathbf{n} \cdot \mathbf{v}) + \mathcal{R}_Q \mathbf{n} \cdot \mathbf{v}] (\mathbf{n}, z_1) [b_\alpha \delta + b_v \mathcal{H}^{-1} \partial_r(\mathbf{n} \cdot \mathbf{v}) + \mathcal{R}_\alpha \mathbf{n} \cdot \mathbf{v}] (\mathbf{n}, z_2) \rangle \\
&\quad - \xi_{Q\alpha}^{\text{newt}} \\
&= \int \frac{dk}{2\pi^2} k^2 P_R(k) j_1(kx) \\
&\quad [b_Q(z_1) \mathcal{R}_\alpha(z_2) T_\delta(k, \eta_1) T_v(k, \eta_2) - \mathcal{R}_Q(z_1) b_\alpha(z_2) T_v(k, \eta_1) T_\delta(k, \eta_2)] \\
&\quad + \int \frac{dk}{2\pi^2} k^3 P_R(k) \left[-\frac{3}{5} j_1(kx) + \frac{2}{5} j_3(kx) \right] \left[\frac{\mathcal{R}_\alpha(z_2)}{\mathcal{H}(z_1)} - \frac{\mathcal{R}_Q(z_1) b_v(z_2)}{\mathcal{H}(z_2)} \right] T_v(k, \eta_1) T_v(k, \eta_2) \\
&\quad + \int \frac{dk}{2\pi^2} k^2 P_R(k) \left[\frac{1}{3} j_0(kx) - \frac{2}{3} j_2(kx) \right] \mathcal{R}_Q(z_1) \mathcal{R}_\alpha(z_2) T_v(k, \eta_1) T_v(k, \eta_2) \tag{4.14}
\end{aligned}$$

with

$$\mathcal{R}_Q = \frac{\dot{\mathcal{H}}}{\mathcal{H}^2} + \frac{2-5s}{r_S \mathcal{H}} + 5s - f_{\text{evo}}^N, \tag{4.15}$$

$$\mathcal{R}_\alpha = -\tau_0 \left(3 + \frac{\dot{\mathcal{H}}}{\mathcal{H}^2} \right), \tag{4.16}$$

and a potential term

$$\begin{aligned}
\xi_{Q\alpha}^{\text{potential}} &\equiv \langle [b_Q \delta + \mathcal{H}^{-1} \partial_r(\mathbf{n} \cdot \mathbf{v}) + \mathcal{R}_Q \mathbf{n} \cdot \mathbf{v} + \mathcal{P}_Q] (\mathbf{n}, z_1) [b_\alpha \delta + b_v \mathcal{H}^{-1} \partial_r(\mathbf{n} \cdot \mathbf{v}) + \mathcal{R}_\alpha \mathbf{n} \cdot \mathbf{v} + \mathcal{P}_\alpha] (\mathbf{n}, z_2) \rangle \\
&\quad - \xi_{Q\alpha}^{\text{newt}} - \xi_{Q\alpha}^{\text{Doppler}} \\
&= \int \frac{dk}{2\pi^2} k^2 P_R(k) j_0(kx) [b_Q(z_1) T_\delta(k, \eta_1) T_{\mathcal{P}_\alpha}(k, \eta_2) + b_\alpha(z_2) T_{\mathcal{P}_Q}(k, \eta_1) T_\delta(k, \eta_2)] \\
&\quad + \int \frac{dk}{2\pi^2} k^3 P_R(k) \left[-\frac{1}{3} j_0(kx) + \frac{2}{3} j_2(kx) \right] \\
&\quad \left[\frac{1}{\mathcal{H}(z_1)} T_v(k, \eta_1) T_{\mathcal{P}_\alpha}(k, \eta_2) + \frac{b_v(z_2)}{\mathcal{H}(z_2)} T_{\mathcal{P}_Q}(k, \eta_1) T_v(k, \eta_2) \right] \\
&\quad + \int \frac{dk}{2\pi^2} k^2 P_R(k) j_1(kx) [\mathcal{R}_Q(z_1) T_v(k, \eta_1) T_{\mathcal{P}_\alpha}(k, \eta_2) - \mathcal{R}_\alpha(z_2) T_{\mathcal{P}_Q}(k, \eta_1) T_v(k, \eta_2)] \\
&\quad + \int \frac{dk}{2\pi^2} k^2 P_R(k) j_0(kx) T_{\mathcal{P}_Q}(k, \eta_1) T_{\mathcal{P}_\alpha}(k, \eta_2) \tag{4.17}
\end{aligned}$$

where we have used the following definitions

$$\mathcal{P}_Q = (5s-2) \Phi + \left(1 + \frac{\dot{\mathcal{H}}}{\mathcal{H}^2} + \frac{2-5s}{r_S \mathcal{H}} + 5s - f_{\text{evo}} \right) \Psi + \mathcal{H}^{-1} \dot{\Phi} + (f_{\text{evo}} - 3) \mathcal{H}v, \tag{4.18}$$

$$\mathcal{P}_\alpha = -\tau_0 \left[\left(3 + \frac{\dot{\mathcal{H}}}{\mathcal{H}^2} \right) \Psi + \mathcal{H}^{-1} \dot{\Phi} - 3\mathcal{H}v \right], \tag{4.19}$$

³For the velocity transfer function $T_v(k, \eta)$ we follow the notation of Ref. [23, 35], namely it refers to vector potential V defined through $\mathbf{v} = i\mathbf{k}V$.

and $T_{\mathcal{P}_Q}$ and $T_{\mathcal{P}_\alpha}$ denote the respective transfer functions normalized with the primordial curvature perturbation. The last term in Eq. (4.13) denotes the contribution of the non-local terms, and their cross-correlation with all the other terms. In particular this includes the correlation between QSO magnification with all (local and non-local) Lyman- α relativistic effects and the correlation between relativistic non-local terms (e.g. ISW, Shapiro time delay) with everything else. Again, as we did for the cosmic magnification we prefer to use Eq. (4.5) to compute them.

4.1 Local term expansion in \mathcal{H}/k

In our derivation we have been as general as possible and our results are valid for any metric theory of gravity provided that photons move along geodesic and photon number is conserved. Since we describe geometrically our observable, the theory of gravity can modify the transfer functions only⁴, as long as the previous assumptions are valid. We have also assumed that sources move along geodesics, but this assumption can be easily relieved. In order to give the flavor of the amplitude in different regimes of the effects previously computed in a relativistic framework, we replace the transfer functions with their counterparts in a 'newtonian' framework. This oversimplification will give us the physical understanding of the effects shown in the next sections. Therefore, we apply the following substitutions

$$T_v(k, \eta) \rightarrow -\frac{\mathcal{H}}{k} f T_\delta(k, \eta) \quad (4.20)$$

$$T_\Psi(k, \eta) \rightarrow -\frac{3}{2} \frac{\mathcal{H}^2}{k^2} \Omega_M T_\delta(k, \eta) \quad (4.21)$$

$$T_\Phi(k, \eta) \rightarrow -\frac{3}{2} \frac{\mathcal{H}^2}{k^2} \Omega_M T_\delta(k, \eta) \quad (4.22)$$

$$T_{\dot{\Phi}}(k, \eta) \rightarrow -\frac{3}{2} \frac{\mathcal{H}^3}{k^2} \Omega_M (f - 1) T_\delta(k, \eta) \quad (4.23)$$

where the growth factor can be approximated in perturbation theory in Λ CDM by $f(z) = \Omega_M(z)^{0.6}$.

By evaluating all the cosmological parameters and biases at the mean redshift z_{mean}

⁴We remark that expressions for bias factors implicitly assume a theory of gravity.

we find

$$\begin{aligned}\xi_{Q\alpha}^{\text{newt}} &\sim b_Q b_\alpha \int \frac{dk}{2\pi^2} k^2 P(k) j_0(kx) \\ &\quad + b_v \int \frac{dk}{2\pi^2} k^2 f^2 P(k) \left[\frac{1}{5} j_0(kx) - \frac{4}{7} j_2(kx) + \frac{8}{35} j_4(kx) \right] \\ &\quad + (b_Q b_v + b_\alpha) \int \frac{dk}{2\pi^2} k^2 f P(k) \left[\frac{1}{3} j_0(kx) - \frac{2}{3} j_2(kx) \right],\end{aligned}\quad (4.24)$$

$$\begin{aligned}\xi_{Q\alpha}^{\text{Doppler}} &\sim (-b_Q \mathcal{R}_\alpha + \mathcal{R}_Q b_\alpha) \int \frac{dk}{2\pi^2} k^2 f P(k) j_1(kx) \frac{\mathcal{H}}{k} \\ &\quad + (-\mathcal{R}_\alpha + \mathcal{R}_Q b_v) \int \frac{dk}{2\pi^2} k^2 f^2 P(k) \left[\frac{3}{5} j_1(kx) - \frac{2}{5} j_3(kx) \right] \frac{\mathcal{H}}{k} \\ &\quad + \mathcal{R}_\alpha \mathcal{R}_Q \int \frac{dk}{2\pi^2} k^2 f^2 P(k) \left[\frac{1}{3} j_0(kx) - \frac{2}{3} j_2(kx) \right] \left(\frac{\mathcal{H}}{k} \right)^2,\end{aligned}\quad (4.25)$$

$$\begin{aligned}\xi_{Q\alpha}^{\text{potentials}} &\sim (b_Q \tilde{\mathcal{P}}_\alpha + \tilde{\mathcal{P}}_Q b_\alpha) \int \frac{dk}{2\pi^2} k^2 P(k) j_0(kx) \left(\frac{\mathcal{H}}{k} \right)^2 \\ &\quad + (\tilde{\mathcal{P}}_\alpha + \tilde{\mathcal{P}}_Q b_v) \int \frac{dk}{2\pi^2} k^2 f P(k) \left[\frac{1}{3} j_0(kx) - \frac{2}{3} j_2(kx) \right] \left(\frac{\mathcal{H}}{k} \right)^2 \\ &\quad + (-\mathcal{R}_Q \tilde{\mathcal{P}}_\alpha + \tilde{\mathcal{P}}_Q \mathcal{R}_\alpha) \int \frac{dk}{2\pi^2} k^2 f P(k) j_1(kx) \left(\frac{\mathcal{H}}{k} \right)^3 \\ &\quad + \tilde{\mathcal{P}}_\alpha \tilde{\mathcal{P}}_Q \int \frac{dk}{2\pi^2} k^2 P_R(k) j_0(kx) \left(\frac{\mathcal{H}}{k} \right)^4\end{aligned}\quad (4.26)$$

where $P(k) = T_\delta(k, \eta)^2 P_R(k)$ denotes the matter power spectrum at the mean redshift. $\tilde{\mathcal{P}}_Q$ and $\tilde{\mathcal{P}}_\alpha$ are the pre-factors defined through the transformations (4.20 - 4.23), namely

$$T_{\mathcal{P}_Q}(k, \eta) \rightarrow \tilde{\mathcal{P}}_Q \frac{\mathcal{H}^2}{k^2} T_\delta(k, \eta), \quad (4.27)$$

$$T_{\mathcal{P}_\alpha}(k, \eta) \rightarrow \tilde{\mathcal{P}}_\alpha \frac{\mathcal{H}^2}{k^2} T_\delta(k, \eta), \quad (4.28)$$

and they can be explicitly computed

$$\tilde{\mathcal{P}}_Q = \frac{3}{2} \Omega_M \left(2 - f + f_{\text{evo}} - \frac{\dot{\mathcal{H}}}{\mathcal{H}^2} + \frac{2f}{3\Omega_M} (3 - f_{\text{evo}}) - 10s + \frac{5s - 2}{\mathcal{H}r} \right), \quad (4.29)$$

$$\tilde{\mathcal{P}}_\alpha = \tau_0 \frac{3}{2} \Omega_M \left(2 + \frac{\dot{\mathcal{H}}}{\mathcal{H}^2} + f - 2 \frac{f}{\Omega_M} \right). \quad (4.30)$$

We remark that the transformation (4.20 - 4.23) has been performed by using Newtonian equations. Nevertheless, it is well known that, for CDM, linearized Einstein equations agree with Newtonian dynamics if perturbations are considered in specific gauges, namely the density perturbation in synchronous gauge and the velocity in Newtonian gauge. Since we have chosen to express perturbations in this combination of

gauges, the expressions here derived include correctly the GR dynamics, as long as the approximation that CDM is the only species which contributes to perturbations is valid.

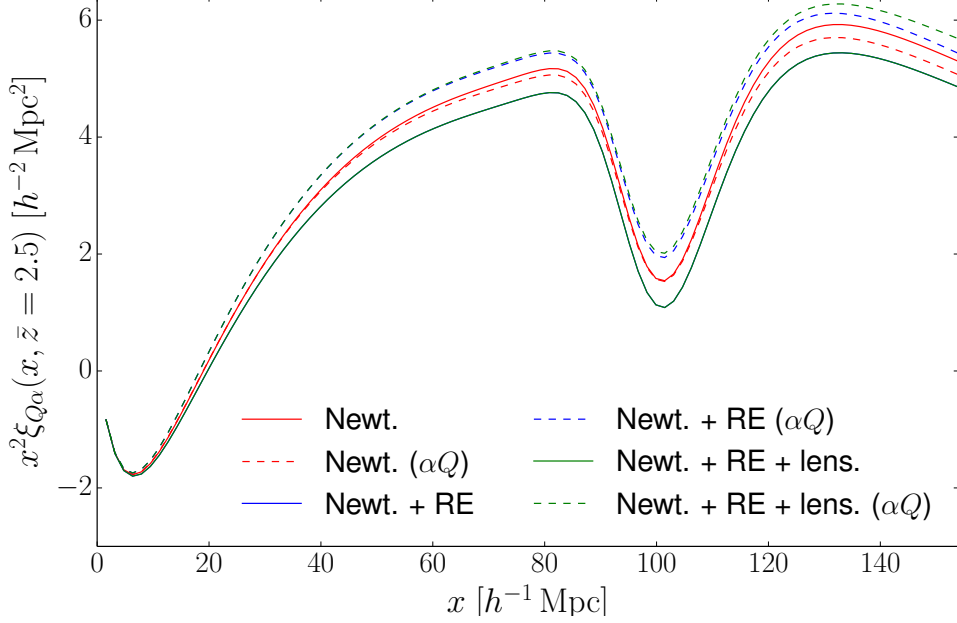


Figure 2. The figure shows the Quasar-Lyman- α cross-correlation function. Different colours correspond to different contributions: red - Newtonian terms (Newt.), blue - Newtonian and relativistic effects (RE), green - Newtonian, relativistic and lensing terms. The full line and dashed line correspond to the cross-correlations $\xi_{Q,\alpha}$ and $\xi_{\alpha,Q}$ respectively. The asymmetry due to the bias evolution, relativistic effects and lensing produce a split of the cross-correlation function around the symmetric part. The dominant effect due to the peculiar velocities of the tracers (Doppler effect) is large on all scales above $20 \text{ h}^{-1} \text{ Mpc}$ while the lensing and redshift evolution effects grow significantly towards larger scales.

According to this scheme, we note that all the newtonian terms contribute at the same parametrical order. The Doppler term, Eq. (4.25), contains the leading correction of order \mathcal{H}/k to the newtonian approximation. This term is non-vanishing only if we use two different tracers or probes. With a single tracer the leading correction would be of the order $(\mathcal{H}/k)^2$, and the amplitude of these terms would be much more suppressed. The leading corrections have also a different parity under the exchange $x \leftrightarrow -x$. Because of that, they contribute only to the antisymmetric part of the correlation function, while newtonian terms (with biases and cosmology evaluated at the mean redshift z_{mean}) lead to a symmetric correlation function only. This argument does not only show the importance of using different probes to try to measure relativistic correction, as already shown in [12, 13, 16], but it also indicates that when we consider cross-correlations between different probes we need to carefully consider effects which might be neglected with a single tracer, as shown in [13, 17]. For simplicity, in this counting scheme we

did not include integrated effects like cosmic magnification, ISW and Shapiro time delay effects. It is known that cosmic magnification can be of the same parametrical order of density and redshift space distortion perturbations, see e.g. [15, 36, 37] and we do include it in the full relativistic analysis in next sections. In the full analysis there is also a contribution to the antisymmetric correlation function due to newtonian terms because of the biases and cosmological parameter evolutions, that have been neglected in this simple approach.

4.2 Symmetric correlation function

The correlation function (4.1) can decompose in a symmetric and anti-symmetric part. In this section we are interested in the symmetric correlation function

$$\xi_{(Q\alpha)}(z_1, z_2, \theta) = \frac{\xi_{Q\alpha}(z_1, z_2, \theta) + \xi_{\alpha Q}(z_1, z_2, \theta)}{2} \quad (4.31)$$

Up to the redshift dependence of transfer functions or bias factors, only the correlation functions which involve even spherical Bessel functions contribute to the symmetric part of the correlation function.

Figure 3 shows the symmetric contribution to the QSO-Lyman- α cross-correlation function. As expected the Newtonian terms (density and RSD) dominate the symmetric signal, while the Relativistic terms (Doppler and potential) only slightly contaminate the result. Similar effect could be observed when one considers only auto-correlations of one tracer. It is interesting to note that while both the Doppler and potential terms in the symmetric form are of the same order of magnitude in the expansion of k ($\sim (\mathcal{H}/k)^2$), the values of the cosmological and bias prefactors are different - mainly the large contribution to the Doppler term comes from the large value of the QSO evolution bias (f_{evo}). Also, while Doppler terms are in general larger than the potential terms, the later become the leading sub-dominant signal at small scales. At very large scales, on the other hand, the lensing terms of the QSO start to become the dominant contaminant. The non-local terms are always small compared to the other effects in the symmetric part of the cross-correlation function. As for the lensing part of the non-local terms, the relative contribution of it grows for large (redshift) separations.

4.3 Anti-symmetric correlation function

Analogously to the symmetric part, we can define the anti-symmetric part of the correlation function

$$\xi_{[Q\alpha]}(z_1, z_2, \theta) = \frac{\xi_{Q\alpha}(z_1, z_2, \theta) - \xi_{\alpha Q}(z_1, z_2, \theta)}{2}. \quad (4.32)$$

A non vanishing anti-symmetric correlation function will indicate a violation of the exchange symmetry of the tracers ($z_1 \leftrightarrow z_2$). Thus, the interchange of the tracers at the same position would produce different results, and which tracer is in the background and which in the foreground would matter. However, this is only true when one is dealing with differently biased tracers. If, for instance, one computes the auto-correlation

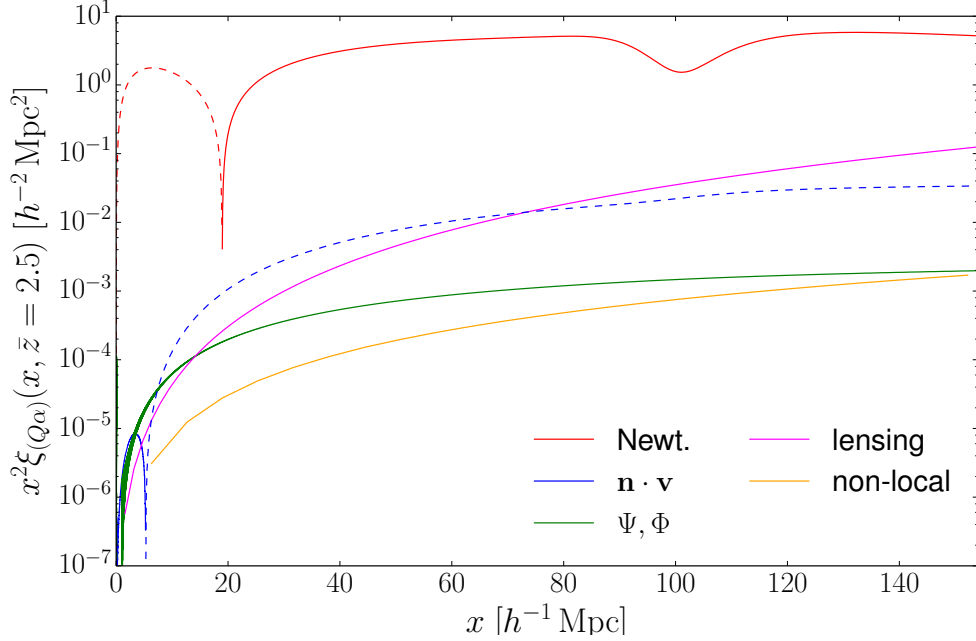


Figure 3. The figure shows the symmetric part of the Quasar-Lyman- α cross-correlation function. Different colours correspond to different contributions: red - Newtonian terms (Newt.), blue - Doppler terms, green - potential terms, magenta - lensing terms and orange - non-local terms. The full line and dashed line correspond to the positive and negative values of the cross-correlations respectively. Newtonian terms dominate the signal in the symmetric part of the cross-correlation function. Note that non-local terms were not computed at very small scales due to numerical issues, however they are very small.

function of one single tracer, the correlation function will be by definition symmetric. On the other hand two different effects can break the symmetry when dealing with different tracers. The asymmetry can come either from different value and redshift evolution of the bias factors or from the intrinsic evolution of the transfer functions. In the case of the galaxy surveys that is the case, and several sources of the asymmetry have been identified and suggested in the literature (e.g. gravitational redshift, Doppler effects, etc.) [12, 16]. These effects reflect the fact that there is not a translation symmetry along the redshift direction, and the asymmetry is generated along the radial direction. Whereas in the angular direction, if statistical isotropy and (angular) homogeneity are not broken, any asymmetry can not be sourced.

Our calculations in the previous sections show that the main source of asymmetry of the correlation functions comes from the Doppler terms in the relativistic expansion (see Fig. 4). In our simple expansion, see Eqs. (4.24, 4.25, 4.26), the Doppler term, Eq. (4.25) contains terms with odd spherical Bessel functions multiplied by only one factor \mathcal{H}/k . In the newtonian term, Eq. (4.24), all the terms are multiplied by even Bessel function, and the asymmetry is generated by the redshift dependence only, while

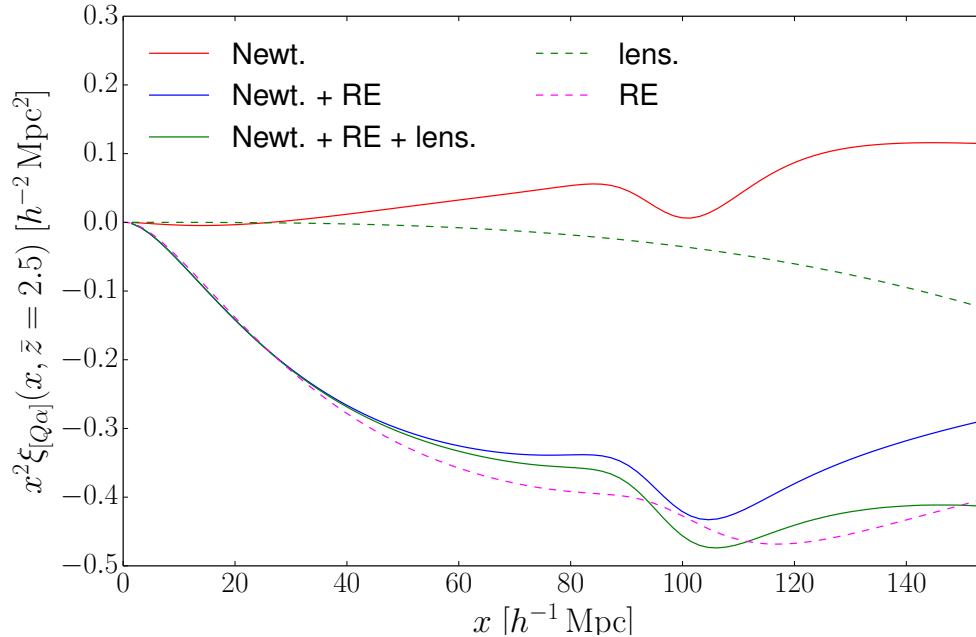


Figure 4. The figure shows different contributions to the anti-symmetric part of the cross-correlation function. Full red line shows the contribution due to the often neglected redshift evolution of the bias factors, dashed magenta line shows the contribution due to the relativistic effects and dashed green line contribution of the lensing terms. The full blue and green lines represent summing up various different terms - redshift evolution and Doppler terms (full blue line), and all the effects (full green line).

in potential term, Eq. (4.26), the terms with odd Bessel function are suppressed by $(\mathcal{H}/k)^3$. The largest single contribution is the Doppler - density correlation which is boosted by the difference in bias factors (see Eq. 4.25). This result is known in the literature and has been commented on at various times, mostly in the context of two galaxy populations [12, 16]. In this paper we have focused on two tracers whose bias factors are as different as possible: quasar bias being very large, and Lyman- α forest flux bias being even negative. Thus ensuring that the signal from the Doppler effect is boosted as much as possible.

The first of the sub-dominant signals is the redshift evolution of the bias factors. Usually one approximates the redshift dependent quantities within a redshift bin with a constant value at the mean redshift. However, redshift evolution of the bias factors gives a fairly large contribution to the asymmetry. This contribution mainly comes from the standard Kaiser terms - indeed one can easily replicate the results by using well known Eq. (4.24) and requiring that the bias factors for quasar and Lyman- α are evaluated not at the mean redshift z_{mean} but at z_1 and z_2 respectively. Strictly speaking, this effect should not be considered for biases only, but for any redshift dependent prefactors

(e.g. cosmological prefactors of the relativistic effects, growth factors, etc.), however in our calculations the effects of growth of structure and evolution of the cosmological parameters (most notably $H(z)$) are very small compared to the other effects, and are well below the 1% of the final result. Thus one can safely use the approximation of constant cosmological parameters evaluated at the mean redshift.

The signal of the bias redshift evolution gives an important contribution, that needs to be modeled if one wants to measure the effects to below 10% accuracy. While it can be regarded as a nuisance signal to the relativistic effects, it requires a precise knowledge of the bias redshift dependence of both tracers. However, this information can be acquired from independent and complementary results, such as auto-correlation functions of each of the tracers, and can be well constrained.

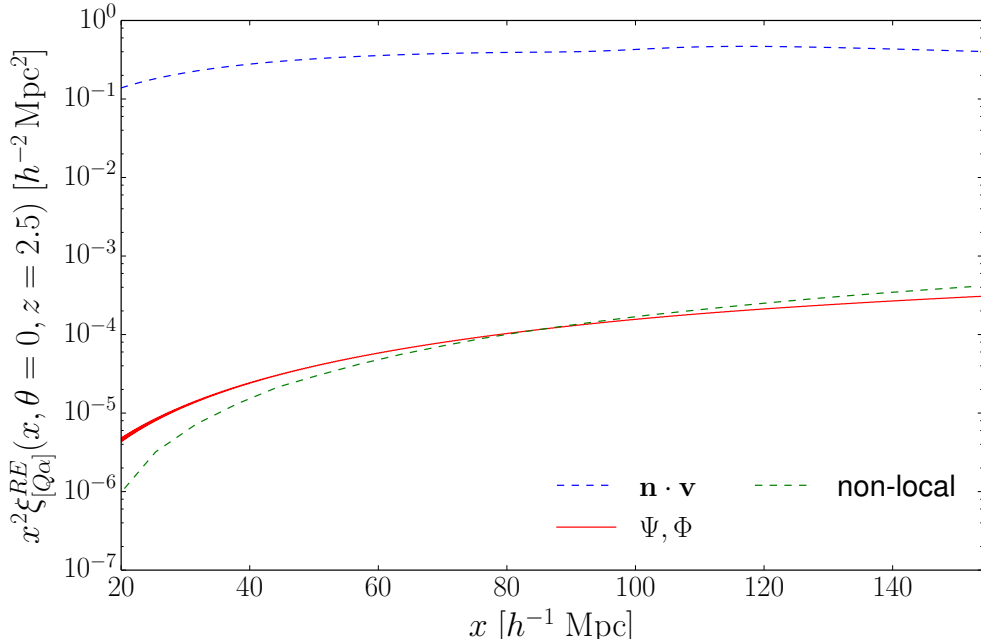


Figure 5. The figure shows different contributions to the relativistic effects in anti-symmetric part of the cross-correlation function. The blue line shows contributions due to the Doppler effects, red line due to potential terms, and green line due to all non-local terms. The difference between full and dashed line is whether the contribution to $\xi_{[Q\alpha]}$ is positive or negative respectively.

Fig. 5 shows the contributions of the relativistic terms to the anti-symmetric part of the $\xi_{Q\alpha}$, broken down into its components. It is clear that at all scales the cross-correlations due to Doppler terms dominate the relativistic signal, while the potential and non-local parts are small.

A special note deserves the fact that all the contaminating effects are small at the BAO scale. This result does not carry any deeper significance, and is a result of the

values of bias factors for the tracers used in this study. Nevertheless, for this particular case it does allow for an easier estimation of the relativistic effects at the BAO scale - which is already a target of many surveys and being a robust feature, very accurately measured.

Figure 6 shows that the signal of the relativistic effects is largest at the BAO scale, compared to the cross-correlation function computed just Newtonian terms. The size of the asymmetry is around 10%, and can reach up to 30% at the BAO scale.

The second contaminating effect is that of the weak lensing signal of quasars. In our specific case the lensing signal can be as large as the effects due to the bias redshift evolution. Similarly to the bias redshift evolution signal, the lensing signal becomes more important on larger scales, and requires careful modeling if one is to measure the overall asymmetry effects to a high precision.

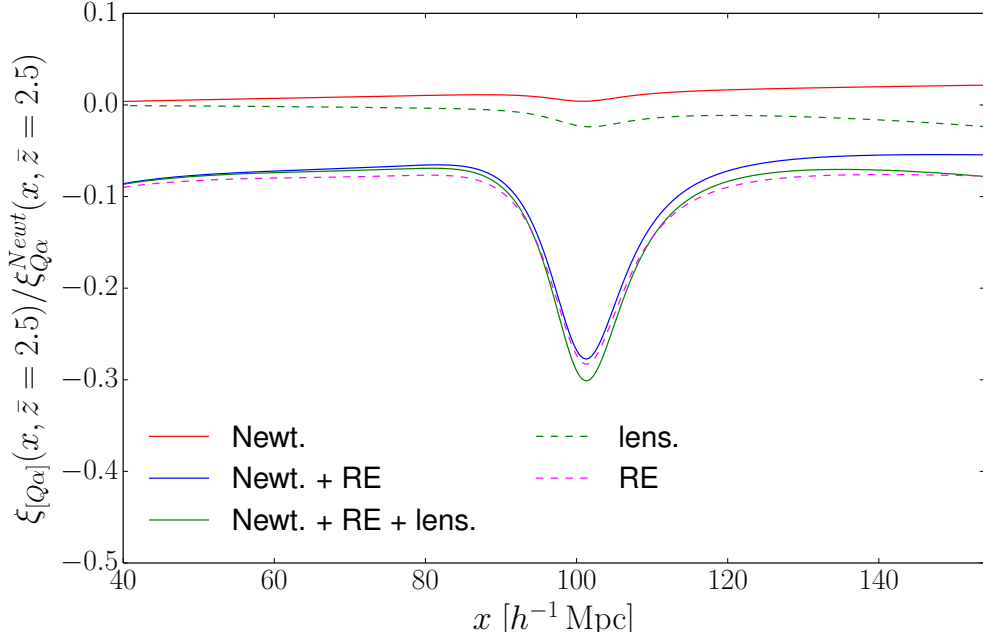


Figure 6. The figure shows the relative size of the anti-symmetric part of the cross-correlation function for different terms. Full red line shows the contribution due to the redshift evolution of the bias factors, dashed magenta line shows the contribution due to the relativistic effects and dashed green line contribution of the lensing terms. The full blue and green lines represent summing up various different terms - redshift evolution and Doppler terms (full blue line), and all the effects (full green line). The relativistic effects can be as large as 30% at the BAO scale, compared to the pure Newtonian calculation (including the bias redshift evolution).

However, the weak lensing effect is proportional to the magnification bias (and on density bias, since the leading term is $\langle \kappa \delta \rangle$), and thus its signal is strongly dependent on this nuisance parameter. We caution that magnification bias needs to be well known, and possibly constrained from independent results, to avoid the contamination of the

signal. The imprecise knowledge of the bias factor affects larger scales the most, it remains important contaminant even at the BAO scales, where it affects the amplitude of the BAO peak, but not its position. Figure 4.3 shows the effects on the asymmetry produced if we change the measured parameters of the Quasar Luminosity Function used to derive the evolution and magnification bias parameters. While the effect of the evolution bias parameter is smaller, it is also degenerate with the effect of the magnification bias at larger scales. However, the change of parameters by 5% shown in the plot is conservative, and future surveys and current surveys will be able to estimate the quasar luminosity function more accurately and hence provide a better estimate on the parameter f_{evo} .

In a standard (single tracer) large scale observable, relativistic effects (except cosmic magnification) are naively suppressed on sub-Hubble scales by the variance induced by the leading newtonian terms and are limited by cosmic variance on large scales. Because of these limitations, all forecasts, see e.g. [13, 14, 17], predict that they are not observable in current and future planned surveys. Nevertheless the antisymmetric correlation function, and more generically the dipole of the 2-point function, represents an independent observable whose leading signal is determined, as we have shown, by relativistic corrections. Hence the detection of relativistic effects is not anymore limited by cosmic variance but it becomes a shot-noise limited observable. Therefore, relativistic effects can be detected on scale much smaller than Hubble size. Not only larger scale experiment, but also advanced data analysis technique like multi-tracers [38], shot-noise canceling [39] and generically correlations between different tracers will probably require to include relativistic effects to correctly interpret the observation and to avoid to introduce any theoretical bias.

5 Conclusions

In this paper we have computed the relativistic effects in the Lyman- α forest in the linear regime on large scales. There are two main reasons to conduct such a study: firstly, the future surveys are going to measure the regime of large scales where the relativistic effects may become important (up to 30% of the signal at the BAO scale), and secondly, the already existing data can be used with multiple tracers to boost specific signals beyond the standard Newtonian terms and constrain cosmological information.

Using two differently biased tracers to boost the small signal of the relativistic effects have been suggested in the past [12, 13, 16, 18, 19] but mostly in the context of different galaxy populations. Here we have adopted the approach, used the newly computed relativistic expansion for the Lyman- α forest and shown that when combining two tracers with very different bias factors (such as Quasars and Lyman- α forest) one can enhance the desired signal.

The main effect on the cross-correlation function can be measured through an asymmetric part of the correlation function. We show that the relativistic effects, and most prominently the Doppler term, give rise to the most dominant contribution. While these new terms include a variety of exciting information, there are two sub-dominant

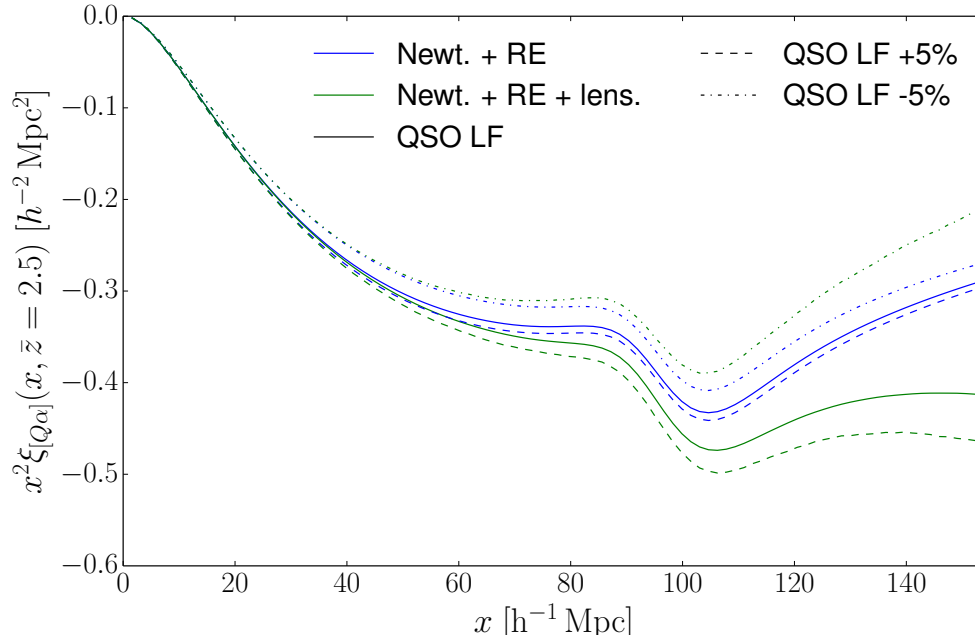


Figure 7. The asymmetry part of the QSO-Lyman- α cross-correlation function. Blue colour represents Newtonian and relativistic terms, while green colour adds lensing to them. The different line shapes correspond to different values of the bias parameters: full line shows the mean values used in our calculations, dashed line shows the values ($s = 0.256883$, $f_{\text{evo}} = 6.19163$) for +5% change to the QSO LF parameters and dot-dashed the values ($s = 0.450115$, $f_{\text{evo}} = 4.74261$) for -5% change to the QSO LF parameters. Even at the BAO scales - the values of the evolution and magnification bias can affect the result by 10% and need to be modeled carefully.

effects that need to be carefully modeled: the redshift evolution of the density (and velocity-gradient) bias factors of the tracers, and the QSO lensing term. In the light of the lensing effects, the cosmological signal is strongly contaminated by the magnification, and to lesser extent, evolution bias of the QSOs. While all the bias parameters can be determined from the independent surveys it is important to note that they can mimic the effects of different cosmology or theory of gravity.

For the given configuration of the tracers the results show that the contaminating effects are surprisingly small at BAO scale. While this only reflects the specific values of the bias parameters and their redshift evolution for these two tracers, it can be used to determine the effect of the Doppler terms at the BAO scale.

Another possible advantage for the precision measurements of future surveys is to isolate the anti-symmetric signal of lensing or potential terms and use them to test the validity of the Einstein's General Relativity or constrain the modifications of the theory of gravity. The dominant signal, coming from the Doppler term, would not change under a different theory of gravity, unless the theory violates the energy-momentum tensor conservation. Even though, the potential and lensing signals are small, if measured they

would provide a unique test of General Relativity on the BAO scales, thus in the regime where perturbations can be measured much better than at horizon scales.

Acknowledgement

We thank Anže Slosar and Ruth Durrer for fruitful discussions. ED and MV are supported by the ERC grant 'cosmoIGM' and by INFN/PD51 INDARK grant.

A Angular power spectrum

After having computed the 2-point correlation function we can compute the power spectrum as well. Since the observables defined in Eqs. (3.17,4.2) depend on angular positions and redshifts, spherical harmonics are the natural basis to expand them as follows

$$\Delta_A(z, \mathbf{n}) = \sum_{\ell m} a_{\ell m}^A(z) Y_{\ell m}(\mathbf{n}) , \quad (\text{A.1})$$

$$a_{\ell m}^A(z) = \int d\Omega_{\mathbf{n}} \Delta_A(z, \mathbf{n}) Y_{\ell m}^*(\mathbf{n}) . \quad (\text{A.2})$$

Then, we define the redshift dependent angular power spectra

$$C_{\ell}^{AB}(z, z') = \langle a_{\ell m}^A(z) a_{\ell m}^{B*}(z') \rangle \quad (\text{A.3})$$

where A and B denotes two observables. It is convenient to write the angular power spectra in terms of integral over the angular transfer function $\Delta_{\ell}^A(\eta, k)$ through

$$C_{\ell}^{AB}(z, z') = 4\pi \int \frac{dk}{k} \Delta_{\ell}^A(k, \eta) \Delta_{\ell}^{B*}(k, \eta') \mathcal{P}_R(k) , \quad (\text{A.4})$$

where $\mathcal{P}_R(k) = k^3 P_R(k) / (2\pi^2)$ is the dimensionless primordial curvature power spectrum. The same formalism has been successfully applied to Cosmic Microwave Background (CMB), Weak Lensing (WL) and galaxy clustering. Because of that, the implementation in a Boltzmann code is straight forward. In this work we have modified the public CLASS code [32, 33], in particular the part included in CLASSgal [35] and we have adopted it to compute, through Eq. (4.5), the correlation function of non-local terms.

As shown in galaxy clustering, the analysis based on redshift dependent 2-dimensional power spectra recovers the same amount of information of the traditional 3-dimensional analysis, see e.g. [15, 40, 41]. In addition, it is the natural way to include relativistic or light-cone effects and it has been already considered in several works. Hence, the formalism here discussed can be used directly to perform a 3-dimensional analysis, including all the relativistic effects to first order in perturbation theory.

Ly- α power transfer function

For the transmitted flux, from Eqs. (3.3, 3.11), we compute the angular transfer function

$$\begin{aligned} \Delta_\ell(k, \eta) = & bT_D j_\ell(kr) + b_v \mathcal{H}^{-1} T_\Theta j_\ell''(kr) \\ & - \tau_0 \left\{ \left[\left(3 + \frac{\dot{\mathcal{H}}}{\mathcal{H}^2} \right) T_\Psi + \mathcal{H}^{-1} T_\Phi - 3 \frac{\mathcal{H}}{k^2} T_\Theta \right] j_\ell(kr) \right. \\ & \left. + \left(3 + \frac{\dot{\mathcal{H}}}{\mathcal{H}^2} \right) k^{-1} T_\Theta j_\ell'(kr) + \left(2 + \frac{\dot{\mathcal{H}}}{\mathcal{H}^2} \right) \int_0^r T_{\dot{\Psi}+\dot{\Phi}} j_\ell(kr') dr' \right\}, \end{aligned} \quad (\text{A.5})$$

where a prime denotes the derivative of the spherical Bessel functions with respect to their argument. All the quantities are evaluated at (k, η) if not written explicitly.

Quasars transfer function

Following the notation of [35], we reproduce here the angular transfer function for QSO

$$\begin{aligned} \Delta_\ell(z, k) = & j_\ell(kr) \left[bT_D + \left(\frac{\dot{\mathcal{H}}}{\mathcal{H}^2} + \frac{2-5s}{r\mathcal{H}} + 5s - f_{\text{evo}}^N + 1 \right) T_\Psi \right. \\ & \left. + (-2+5s) T_\Phi + \mathcal{H}^{-1} T_\dot{\Phi} \right] \\ & + \left[\frac{dj_\ell}{dx}(kr) \left(\frac{\dot{\mathcal{H}}}{\mathcal{H}^2} + \frac{2-5s}{r\mathcal{H}} + 5s - f_{\text{evo}}^N \right) + \frac{d^2 j_\ell}{dx^2}(kr) \frac{k}{\mathcal{H}} (f_{\text{evo}} - 3) j_\ell(kr) \frac{\mathcal{H}}{k} \right] T_V \\ & + \int_0^{r(z)} dr j_\ell(kr) \left[T_{\Phi+\Psi} \left(\frac{2-5s}{2} \right) \left(\ell(\ell+1) \frac{r(z)-r}{r(z)r} + \frac{2}{r(z)} \right) \right. \\ & \left. + T_{\dot{\Phi}+\dot{\Psi}} \left(\frac{\dot{\mathcal{H}}}{\mathcal{H}^2} + \frac{2-5s}{r(z)\mathcal{H}} + 5s - f_{\text{evo}}^N \right)_{r(z)} \right]. \end{aligned} \quad (\text{A.6})$$

B CLASS modifications

Here we present the modified transfer function in CLASS code [32, 33], in particular for the galaxy number counts calculation developed in CLASSgal [35]

$$c_\ell^{ij} = 4\pi \int \frac{dk}{k} \mathcal{P}_{\mathcal{R}}(k) \Delta_\ell^i(k) \Delta_\ell^j(k) \quad (\text{B.1})$$

where

$$\begin{aligned} \Delta_\ell(k) = & \Delta_\ell^{\text{Den}_i} && (\text{Density}) \\ & + \Delta_\ell^{\text{Red}_i} && (\text{Redshift space distortion}) \\ & + \Delta_\ell^{\text{D1}_i} + \Delta_\ell^{\text{D2}_i} && (\text{Doppler}) \\ & + \Delta_\ell^{\text{G1}_i} + \Delta_\ell^{\text{G2}_i} + \Delta_\ell^{\text{G3}_i} + \Delta_\ell^{\text{G5}_i} && (\text{Gravitational potential}) \end{aligned} \quad (\text{B.2})$$

With

$$\begin{aligned}
\Delta_\ell^{\text{Den}_i} &= \int_0^{\eta_0} d\eta W_i b_{\text{SD}} j_\ell \\
\Delta_\ell^{\text{Red}_i} &= \int_0^{\eta_0} d\eta W_i \frac{b_v}{aH} S_\Theta \frac{d^2 j_\ell}{dx^2} \\
\Delta_\ell^{\text{D1}_i} &= - \int_0^{\eta_0} d\eta W_i \frac{4 + \frac{\dot{H}}{aH^2}}{k} S_\Theta \tau_0 \frac{dj_\ell}{dx} \\
\Delta_\ell^{\text{D2}_i} &= \int_0^{\eta_0} d\eta W_i 3 \frac{aH}{k^2} S_\Theta \tau_0 j_\ell \\
\Delta_\ell^{\text{G1}_i} &= - \int_0^{\eta_0} d\eta W_i S_\Psi \tau_0 j_\ell \\
\Delta_\ell^{\text{G2}_i} &= \int_0^{\eta_0} d\eta W_i \left(3 + \frac{\dot{H}}{aH^2} \right) S_\Phi \tau_0 j_\ell \\
\Delta_\ell^{\text{G3}_i} &= - \int_0^{\eta_0} d\eta W_i \frac{1}{aH} S_\Phi \tau_0 j_\ell \\
\Delta_\ell^{\text{G5}_i} &= \int_0^{\eta_0} d\eta W_i^{\text{G5}} S_{(\Phi+\Psi)} k \frac{dj_\ell}{dx} .
\end{aligned} \tag{B.3}$$

We have omitted all the arguments: k for the transfer functions, (η, k) for the source functions, $x \equiv k(\eta_0 - \eta)$ for the Bessel functions, and η for selection and background functions. For the integrated term G5, we have defined

$$W_i^{\text{G5}}(\eta) = - \int_0^\eta d\tilde{\eta} \tau_0 W_i(\tilde{\eta}) \left(3 + \frac{\dot{H}}{aH^2} \right)_{\tilde{\eta}} .$$

The term G4 vanishes because of the absence of time-delay effect in Lyman- α observable.

References

- [1] M. Rauch, *The Lyman Alpha Forest in the Spectra of QSOs*, ARAA **36** (1998) 267–316, [[astro-ph/9806286](#)].
- [2] A. A. Meiksin, *The physics of the intergalactic medium*, Reviews of Modern Physics **81** (Oct., 2009) 1405–1469, [[arXiv:0711.3358](#)].
- [3] N. G. Busca, T. Delubac, J. Rich, S. Bailey, A. Font-Ribera, D. Kirkby, J.-M. Le Goff, M. M. Pieri, A. Slosar, É. Aubourg, J. E. Bautista, D. Bizyaev, M. Blomqvist, A. S. Bolton, J. Bovy, H. Brewington, A. Borde, J. Brinkmann, B. Carithers, R. A. C. Croft, K. S. Dawson, G. Ebelke, D. J. Eisenstein, J.-C. Hamilton, S. Ho, D. W. Hogg, K. Honscheid, K.-G. Lee, B. Lundgren, E. Malanushenko, V. Malanushenko, D. Margala, C. Maraston, K. Mehta, J. Miralda-Escudé, A. D. Myers, R. C. Nichol, P. Noterdaeme, M. D. Olmstead, D. Oravetz, N. Palanque-Delabrouille, K. Pan, I. Pâris, W. J. Percival, P. Petitjean, N. A. Roe, E. Rollinde, N. P. Ross, G. Rossi, D. J. Schlegel, D. P. Schneider, A. Sheldon, E. S. Sheldon, A. Simmons, S. Snedden, J. L. Tinker, M. Viel, B. A. Weaver, D. H. Weinberg, M. White, C. Yèche, and D. G. York, *Baryon acoustic oscillations in the Ly α forest of BOSS quasars*, A&A **552** (Apr., 2013) A96, [[arXiv:1211.2616](#)].

- [4] A. Slosar, V. Iršič, D. Kirkby, S. Bailey, N. G. Busca, T. Delubac, J. Rich, É. Aubourg, J. E. Bautista, V. Bhardwaj, M. Blomqvist, A. S. Bolton, J. Bovy, J. Brownstein, B. Carithers, R. A. C. Croft, K. S. Dawson, A. Font-Ribera, J.-M. Le Goff, S. Ho, K. Honscheid, K.-G. Lee, D. Margala, P. McDonald, B. Medolin, J. Miralda-Escudé, A. D. Myers, R. C. Nichol, P. Noterdaeme, N. Palanque-Delabrouille, I. Pâris, P. Petitjean, M. M. Pieri, Y. Piškur, N. A. Roe, N. P. Ross, G. Rossi, D. J. Schlegel, D. P. Schneider, N. Suzuki, E. S. Sheldon, U. Seljak, M. Viel, D. H. Weinberg, and C. Yèche, *Measurement of baryon acoustic oscillations in the Lyman- α forest fluctuations in BOSS data release 9*, *JCAP* **4** (Apr., 2013) 26, [[arXiv:1301.3459](#)].
- [5] N. Palanque-Delabrouille, C. Yèche, A. Borde, J.-M. Le Goff, G. Rossi, M. Viel, É. Aubourg, S. Bailey, J. Bautista, M. Blomqvist, A. Bolton, J. S. Bolton, N. G. Busca, B. Carithers, R. A. C. Croft, K. S. Dawson, T. Delubac, A. Font-Ribera, S. Ho, D. Kirkby, K.-G. Lee, D. Margala, J. Miralda-Escudé, D. Muna, A. D. Myers, P. Noterdaeme, I. Pâris, P. Petitjean, M. M. Pieri, J. Rich, E. Rollinde, N. P. Ross, D. J. Schlegel, D. P. Schneider, A. Slosar, and D. H. Weinberg, *The one-dimensional Ly α forest power spectrum from BOSS*, *A&A* **559** (Nov., 2013) A85, [[arXiv:1306.5896](#)].
- [6] N. Palanque-Delabrouille, C. Yèche, J. Baur, C. Magneville, G. Rossi, J. Lesgourgues, A. Borde, E. Burtin, J.-M. LeGoff, J. Rich, M. Viel, and D. Weinberg, *Cosmology with Lyman-alpha forest power spectrum*, *ArXiv e-prints* (June, 2015) [[arXiv:1506.0597](#)].
- [7] M. Viel, G. D. Becker, J. S. Bolton, and M. G. Haehnelt, *Warm dark matter as a solution to the small scale crisis: New constraints from high redshift Lyman- α forest data*, *Phys. Rev. D* **88** (Aug., 2013) 043502, [[arXiv:1306.2314](#)].
- [8] A. Font-Ribera, J. Miralda-Escudé, E. Arnau, B. Carithers, K.-G. Lee, P. Noterdaeme, I. Pâris, P. Petitjean, J. Rich, E. Rollinde, N. P. Ross, D. P. Schneider, M. White, and D. G. York, *The large-scale cross-correlation of Damped Lyman alpha systems with the Lyman alpha forest: first measurements from BOSS*, *JCAP* **11** (Nov., 2012) 59, [[arXiv:1209.4596](#)].
- [9] A. Font-Ribera, E. Arnau, J. Miralda-Escudé, E. Rollinde, J. Brinkmann, J. R. Brownstein, K.-G. Lee, A. D. Myers, N. Palanque-Delabrouille, I. Pâris, P. Petitjean, J. Rich, N. P. Ross, D. P. Schneider, and M. White, *The large-scale quasar-Lyman α forest cross-correlation from BOSS*, *JCAP* **5** (May, 2013) 18, [[arXiv:1303.1937](#)].
- [10] K. S. Dawson, J.-P. Kneib, W. J. Percival, S. Alam, F. D. Albareti, S. F. Anderson, E. Armengaud, E. Aubourg, S. Bailey, J. E. Bautista, A. A. Berlind, M. A. Bershad, F. Beutler, D. Bizyaev, M. R. Blanton, M. Blomqvist, A. S. Bolton, J. Bovy, W. N. Brandt, J. Brinkmann, J. R. Brownstein, E. Burtin, N. G. Busca, Z. Cai, C.-H. Chuang, N. Clerc, J. Comparat, F. Cope, R. A. C. Croft, I. Cruz-Gonzalez, L. N. da Costa, M.-C. Cousinou, J. Darling, S. de la Torre, T. Delubac, H. du Mas des Bourboux, T. Dwelly, A. Ealet, D. J. Eisenstein, M. Eracleous, S. Escoffier, X. Fan, A. Finoguenov, A. Font-Ribera, P. Frinchaboy, P. Gaulme, A. Georgakakis, P. Green, H. Guo, J. Guy, S. Ho, D. Holder, J. Huehnerhoff, T. Hutchinson, Y. Jing, E. Jullo, V. Kamble, K. Kinemuchi, D. Kirkby, F.-S. Kitaura, M. A. Klaene, R. R. Laher, D. Lang, P. Laurent, J.-M. Le Goff, C. Li, Y. Liang, M. Lima, Q. Lin, W. Lin, Y.-T. Lin, D. C. Long, B. Lundgren, N. MacDonald, M. A. Geimba Maia, E. Malanushenko, V. Malanushenko, V. Mariappan, C. K. McBride, I. D. McGreer, B. Menard, A. Merloni, A. Meza, A. D. Montero-Dorta, D. Muna, A. D. Myers, K. Nandra, T. Naugle, J. A. Newman, P. Noterdaeme, P. Nugent, R. Ogando, M. D. Olmstead, A. Oravetz, D. J. Oravetz,

- N. Padmanabhan, N. Palanque-Delabrouille, K. Pan, J. K. Parejko, I. Paris, J. A. Peacock, P. Petitjean, M. M. Pieri, A. Pisani, F. Prada, A. Prakash, A. Raichoor, B. Reid, J. Rich, J. Ridl, S. Rodriguez-Torres, A. Carnero Rosell, A. J. Ross, G. Rossi, J. Ruan, M. Salvato, C. Sayres, D. P. Schneider, D. J. Schlegel, U. Seljak, H.-J. Seo, B. Sesar, S. Shandera, Y. Shu, A. Slosar, F. Sobreira, M. A. Strauss, A. Streblyanska, N. Suzuki, C. Tao, J. L. Tinker, R. Tojeiro, M. Vargas-Magana, Y. Wang, B. A. Weaver, D. H. Weinberg, M. White, W. M. Wood-Vasey, C. Yeche, Z. Zhai, C. Zhao, G.-b. Zhao, Z. Zheng, G. Ben Zhu, and H. Zou, *The SDSS-IV extended Baryon Oscillation Spectroscopic Survey: Overview and Early Data*, ArXiv e-prints (Aug., 2015) [[arXiv:1508.0447](#)].
- [11] M. Levi, C. Bebek, T. Beers, R. Blum, R. Cahn, D. Eisenstein, B. Flaugher, K. Honscheid, R. Kron, O. Lahav, P. McDonald, N. Roe, D. Schlegel, and representing the DESI collaboration, *The DESI Experiment, a whitepaper for Snowmass 2013*, ArXiv e-prints (Aug., 2013) [[arXiv:1308.0847](#)].
- [12] P. McDonald, *Gravitational redshift and other redshift-space distortions of the imaginary part of the power spectrum*, JCAP **0911** (2009) 026, [[arXiv:0907.5220](#)].
- [13] J. Yoo, N. Hamaus, U. Seljak, and M. Zaldarriaga, *Going beyond the Kaiser redshift-space distortion formula: a full general relativistic account of the effects and their detectability in galaxy clustering*, Phys. Rev. **D86** (2012) 063514, [[arXiv:1206.5809](#)].
- [14] J. Yoo and U. Seljak, *Wide Angle Effects in Future Galaxy Surveys*, Mon. Not. Roy. Astron. Soc. **447** (2015), no. 2 1789–1805, [[arXiv:1308.1093](#)].
- [15] E. Di Dio, F. Montanari, R. Durrer, and J. Lesgourgues, *Cosmological Parameter Estimation with Large Scale Structure Observations*, JCAP **1401** (2014) 042, [[arXiv:1308.6186](#)].
- [16] C. Bonvin, L. Hui, and E. Gaztanaga, *Asymmetric galaxy correlation functions*, Phys. Rev. **D89** (2014), no. 8 083535, [[arXiv:1309.1321](#)].
- [17] D. Alonso, P. Bull, P. G. Ferreira, R. Maartens, and M. G. Santos, *Ultra-large scale cosmology with next-generation experiments*, [arXiv:1505.0759](#).
- [18] D. Alonso and P. G. Ferreira, *Constraining ultra large-scale cosmology with multiple tracers in optical and radio surveys*, [arXiv:1507.0355](#).
- [19] J. Fonseca, S. Camera, M. Santos, and R. Maartens, *Hunting down horizon-scale effects with multi-wavelength surveys*, [arXiv:1507.0460](#).
- [20] A. Arinyo-i-Prats, J. Miralda-Escudé, M. Viel, and R. Cen, *The Non-Linear Power Spectrum of the Lyman Alpha Forest*, ArXiv e-prints (June, 2015) [[arXiv:1506.0451](#)].
- [21] A. Slosar, A. Font-Ribera, M. M. Pieri, J. Rich, J.-M. Le Goff, É. Aubourg, J. Brinkmann, N. Busca, B. Carithers, R. Charlassier, M. Cortès, R. Croft, K. S. Dawson, D. Eisenstein, J.-C. Hamilton, S. Ho, K.-G. Lee, R. Lupton, P. McDonald, B. Medolin, D. Muna, J. Miralda-Escudé, A. D. Myers, R. C. Nichol, N. Palanque-Delabrouille, I. Pâris, P. Petitjean, Y. Piškur, E. Rollinde, N. P. Ross, D. J. Schlegel, D. P. Schneider, E. Sheldon, B. A. Weaver, D. H. Weinberg, C. Yeche, and D. G. York, *The Lyman- α forest in three dimensions: measurements of large scale flux correlations from BOSS 1st-year data*, JCAP **9** (Sept., 2011) 1, [[arXiv:1104.5244](#)].
- [22] P. McDonald, *Toward a Measurement of the Cosmological Geometry at $z \sim 2$: Predicting*

- Ly α Forest Correlation in Three Dimensions and the Potential of Future Data Sets*, *ApJ* **585** (Mar., 2003) 34–51, [[astro-ph/0108064](#)].
- [23] C. Bonvin and R. Durrer, *What galaxy surveys really measure*, *Phys. Rev.* **D84** (2011) 063505, [[arXiv:1105.5280](#)].
 - [24] **Planck** Collaboration, P. A. R. Ade et al., *Planck 2015 results. XIII. Cosmological parameters*, [arXiv:1502.0158](#).
 - [25] U. Seljak, *Bias, redshift space distortions and primordial nongaussianity of nonlinear transformations: application to Ly- α forest*, *JCAP* **3** (Mar., 2012) 4, [[arXiv:1201.0594](#)].
 - [26] P. McDonald, U. Seljak, S. Burles, D. J. Schlegel, D. H. Weinberg, R. Cen, D. Shih, J. Schaye, D. P. Schneider, N. A. Bahcall, J. W. Briggs, J. Brinkmann, R. J. Brunner, M. Fukugita, J. E. Gunn, Ž. Ivezić, S. Kent, R. H. Lupton, and D. E. Vanden Berk, *The Ly α Forest Power Spectrum from the Sloan Digital Sky Survey*, *ApJS* **163** (Mar., 2006) 80–109, [[astro-ph/0405013](#)].
 - [27] A. Challinor and A. Lewis, *The linear power spectrum of observed source number counts*, *Phys. Rev.* **D84** (2011) 043516, [[arXiv:1105.5292](#)].
 - [28] N. P. Ross, I. D. McGreer, M. White, G. T. Richards, A. D. Myers, N. Palanque-Delabrouille, M. A. Strauss, S. F. Anderson, Y. Shen, W. N. Brandt, C. Yèche, M. E. C. Swanson, É. Aubourg, S. Bailey, D. Bizyaev, J. Bovy, H. Brewington, J. Brinkmann, C. DeGraf, T. Di Matteo, G. Ebelke, X. Fan, J. Ge, E. Malanushenko, V. Malanushenko, R. Mandelbaum, C. Maraston, D. Muna, D. Oravetz, K. Pan, I. Pâris, P. Petitjean, K. Schawinski, D. J. Schlegel, D. P. Schneider, J. D. Silverman, A. Simmons, S. Snedden, A. Streblyanska, N. Suzuki, D. H. Weinberg, and D. York, *The SDSS-III Baryon Oscillation Spectroscopic Survey: The Quasar Luminosity Function from Data Release Nine*, *ApJ* **773** (Aug., 2013) 14, [[arXiv:1210.6389](#)].
 - [29] S. M. Croom, B. J. Boyle, T. Shanks, R. J. Smith, L. Miller, P. J. Outram, N. S. Loaring, F. Hoyle, and J. da Ângela, *The 2dF QSO Redshift Survey - XIV. Structure and evolution from the two-point correlation function*, *MNRAS* **356** (Jan., 2005) 415–438, [[astro-ph/0409314](#)].
 - [30] A. D. Myers, R. J. Brunner, R. C. Nichol, G. T. Richards, D. P. Schneider, and N. A. Bahcall, *Clustering Analyses of 300,000 Photometrically Classified Quasars. I. Luminosity and Redshift Evolution in Quasar Bias*, *ApJ* **658** (Mar., 2007) 85–98, [[astro-ph/0612190](#)].
 - [31] M. White, A. D. Myers, N. P. Ross, D. J. Schlegel, J. F. Hennawi, Y. Shen, I. McGreer, M. A. Strauss, A. S. Bolton, J. Bovy, X. Fan, J. Miralda-Escude, N. Palanque-Delabrouille, I. Paris, P. Petitjean, D. P. Schneider, M. Viel, D. H. Weinberg, C. Yèche, I. Zehavi, K. Pan, S. Snedden, D. Bizyaev, H. Brewington, J. Brinkmann, V. Malanushenko, E. Malanushenko, D. Oravetz, A. Simmons, A. Sheldon, and B. A. Weaver, *The clustering of intermediate-redshift quasars as measured by the Baryon Oscillation Spectroscopic Survey*, *MNRAS* **424** (Aug., 2012) 933–950, [[arXiv:1203.5306](#)].
 - [32] J. Lesgourgues, *The Cosmic Linear Anisotropy Solving System (CLASS) I: Overview*, [arXiv:1104.2932](#).
 - [33] D. Blas, J. Lesgourgues, and T. Tram, *The Cosmic Linear Anisotropy Solving System (CLASS) II: Approximation schemes*, *JCAP* **1107** (2011) 034, [[arXiv:1104.2933](#)].
 - [34] M. LoVerde and N. Afshordi, *Extended Limber Approximation*, *Phys. Rev.* **D78** (2008) 123506, [[arXiv:0809.5112](#)].

- [35] E. Di Dio, F. Montanari, J. Lesgourgues, and R. Durrer, *The CLASSgal code for Relativistic Cosmological Large Scale Structure*, JCAP **1311** (2013) 044, [[arXiv:1307.1459](#)].
- [36] A. Raccañelli, D. Bertacca, R. Maartens, C. Clarkson, and O. Doré, *Lensing and time-delay contributions to galaxy correlations*, [arXiv:1311.6813](#).
- [37] F. Montanari and R. Durrer, *Measuring the lensing potential with galaxy clustering*, [arXiv:1506.0136](#).
- [38] U. Seljak, *Extracting primordial non-gaussianity without cosmic variance*, Phys. Rev. Lett. **102** (2009) 021302, [[arXiv:0807.1770](#)].
- [39] U. Seljak, N. Hamaus, and V. Desjacques, *How to suppress the shot noise in galaxy surveys*, Phys. Rev. Lett. **103** (2009) 091303, [[arXiv:0904.2963](#)].
- [40] J. Asorey, M. Crocce, E. Gaztanaga, and A. Lewis, *Recovering 3D clustering information with angular correlations*, Mon. Not. Roy. Astron. Soc. **427** (2012) 1891, [[arXiv:1207.6487](#)].
- [41] A. Nicola, A. Refregier, A. Amara, and A. Paranjape, *Three-dimensional spherical analyses of cosmological spectroscopic surveys*, Phys. Rev. **D90** (2014), no. 6 063515, [[arXiv:1405.3660](#)].